

Paper:

Study on Performance Evaluation of MEMS Sensors and Data Integration Methods for Expected Use to Determine Damage Degrees of Existing Structures

Tomohiro Sasaki[†], Koichi Kajiwara, Takuzo Yamashita, and Takuya Toyoshi

National Research Institute for Earth Science and Disaster Resilience (NIED)

1501-21 Mitsuta, Shijimi-cho, Miki, Hyogo 673-0515, Japan

[†]Corresponding author, E-mail: tomo_s@bosai.go.jp

[Received April 14, 2017; accepted July 12, 2017]

The shake table test of small-scaled steel frame structure was conducted using large-scale earthquake simulator at the National Research Institute for Earth Science and Disaster Resilience (NIED) in Tsukuba, Ibaragi. This paper presents the performance evaluation of Micro Electro Mechanical Systems (MEMS) type accelerometers, which are recently being used in various fields, comparing with the conventional servo type accelerometers. In addition, this paper discussed the integration method of the measured acceleration into displacements, which is suitable for structural damage evaluation due to strong earthquakes.

Keywords: micro electro mechanical systems (MEMS), shake table test, accelerometer, steel structure

1. Introduction

Over the past nearly 20 years, great earthquakes such as the 1995 Kobe earthquake, the 2011 Tohoku earthquake and the 2016 Kumamoto earthquake occurred and a lot of structures suffered significant damage or collapsed. Even though the structure does not collapse, the risk of collapse and residual strength of it must be evaluated and judge of evacuation is needed. However, this judge requires the professional knowledge and experience on structural engineering and thus is difficult for general users and administrators. Recently, in order to cope with this problem, several studies on development of automatic structural damage evaluation method were conducted using networks of various kinds of sensors to measure the response of structures during strong earthquake (e.g., [1–3]).

Accelerometers are generally used to measure the response of structures during an earthquake. As accelerations are a common indicator of vibrations, loads that act on structures can be easily obtained by multiplying accelerations by masses. Accelerometers are widely used because they do not require any special equipment to measure vibrations.

However, the occurrence of damages to structures is closely linked to the deformation of structural members.

Thus, displacements are often used to evaluate the damage level of structures. For measuring displacements, a rigid frame structure is required as a reference point. Generally, members of the rigid reference frame have large and stiff enough cross sections, so as not to affect measurements. The rigid reference frame is usually designed to have a high natural frequency, which is more than ten times higher than natural frequency of target structures. As the rigid reference frame becomes larger, however, it will become more difficult to achieve the high natural frequency mentioned above. Therefore, the acceleration measurement, which can measure absolute accelerations only by installing accelerometers, is much easier measuring method than the displacement measurement.

To obtain the displacement for evaluation of the damage of structures, double integration of the acceleration can be used. The drift components generated by the measuring errors, noises, and permanent displacements, among other factors, are so greatly amplified in the integration process that the integration results becomes unrealistic response. Therefore, baseline correction [4] or low-cut filter [5] is widely used.

Most of the sensors used to measure accelerations in the past were of strain, servo, or piezoelectric types, which directly output analog electric signals in proportion to the accelerations (analog sensors). Recently, however, as the semiconductor technology has been developed, greatly advancing the micromachining technology on silicon and other substrates, accelerometers of micro electro mechanical systems (MEMS) type are more widely used. MEMS type sensors, though slightly inferior in accuracy compared to the conventional sensors, are small size, light weight, low in power consumption, and high in affinity to IC, and can directly output digital signals when built on IC. Further, they can be mounted on a variety of digital devices, such as mobile phones, to detect their inclinations.

Such MEMS type accelerometers are in many cases less expensive than conventional analog sensors, and recent technological developments have improved their accuracy to the point where it is now nearly equal to that of the conventional sensors. MEMS type accelerometers, which are often mounted not only as accelerometers but



also as gyro sensors capable of measuring angular velocities, can collect more information. Hence, they present a very promising outlook.

As we plan in our future studies to promote the use of MEMS type accelerometers for structural health monitoring of existing structures, this paper presents the performance evaluation of the MEMS type accelerometers and discuss integration of acceleration. In Section 2, the performance of the MEMS type accelerometers is evaluated based on the shake table test of the small-scaled steel frame structure using large uniaxial shake table named “Large scale earthquake simulator” belonging to the National Research Institute for Earth Science and Disaster Resilience (NIED). In Section 3, the suitable integration method for structural health monitoring is discussed.

2. Performance Evaluation of MEMS Sensors based on a Shake Table Test of Small-Scaled Steel Frame Structure

2.1. Small-Scaled Steel Frame Specimen and Excitation Plans

Figure 1 shows a small-scaled steel frame specimen. The specimen is directly fixed on the shake table and excited in the long-side direction. Hereinafter, in the coordinated axes, the long-side direction is denoted by X, the short-side direction by Y, and the vertical direction by Z. The objective of this experiment is collecting data to improve accuracy of numerical simulation for evaluation of residual strength of structures [6].

The specimen is a one-third scaled model of the two lower floors of a typical four-story steel building. Span is 4000 mm in the X-direction, 2000 mm in the Y-direction, and height of specimen is 2744 mm. To simulate the dead load in each floor, a 6.79 ton weight is loaded in each floor. Total weight of the specimen is 14.57 ton.

The artificial record provided by the Building Center in Japan is used as imposed motion. This record is one of the typical design level 2 ground acceleration record in Japan (designated as BCJ-L2 record, hereinafter). Because the specimen is 1/3 scaled model, time scale of the record is reduced in $1/\sqrt{3}$ to achieve similarity law. The amplitude of imposed motion is gradually increased from 40% to 270%, until the specimen completely collapsed.

To measure the responses of the specimen, servo type 3-axial accelerometers TA-25E manufactured by TOKYO KEIKI and MEMS type 6-axis acceleration/gyro sensors M-G550PC20 manufactured by EPSON are installed at the column base, connections, center of the beam, and on the top of the weight. Wire type displacement transducers are also installed at the connection reference from the rigid frame close to the specimen. **Fig. 2** shows the locations of the sensors mentioned above. The sampling rates are 1000 Hz for the servo type accelerometers and wire type displacement transducers, and 500 Hz for the MEMS type acceleration/gyro sensors. 1000 Hz analog filters for the measurements by the servo type accelerom-



Fig. 1. Small-scaled steel frame specimen.

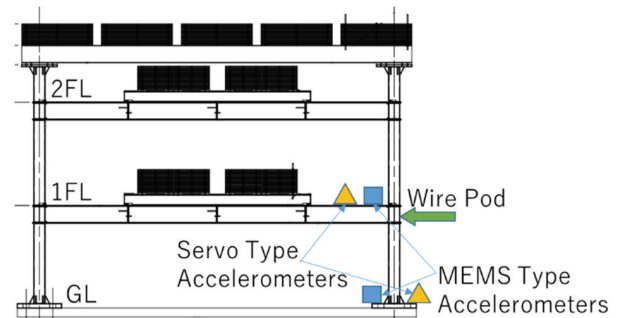


Fig. 2. Locations of sensors.

Table 1. Specification of acceleration/gyro sensors.

		TA-25J	M-G550PC20
Type		Servo	MEMS
Accelerometer	Range	10 G	5 G
	Measurable Frequency Range	450 Hz	200 Hz
	Sensitivity	10^{-6} G	2×10^{-4} G
Gyro	Range	N/A	150 deg/s
	Measurable Frequency Range		200 Hz
	Sensitivity		8×10^{-3} deg/s

eters and wire type displacement transducers, and moving average filters of two sampling points for the MEMS type acceleration/gyro sensors are used. **Table 1** lists the specifications of the acceleration/gyro sensors we have used.

2.2. Performance of MEMS Type Accelerometers

Figure 3 shows the accelerations as measured by the MEMS type and servo type accelerometers, both installed on 1FL, in response by 40% of the BCJ-L2 record. **Fig. 4** shows the power spectrum densities (PSD) of the mea-

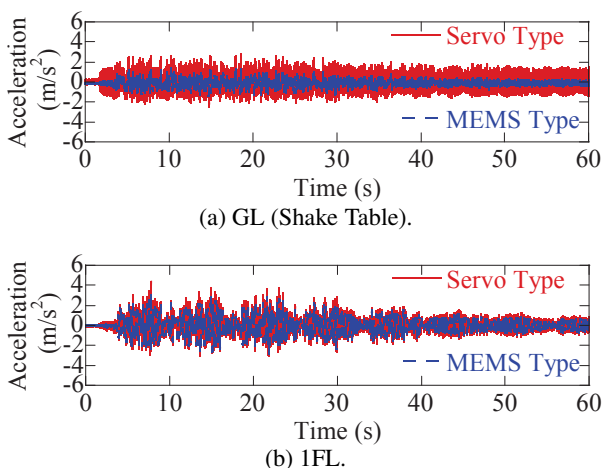


Fig. 3. Measured accelerations.

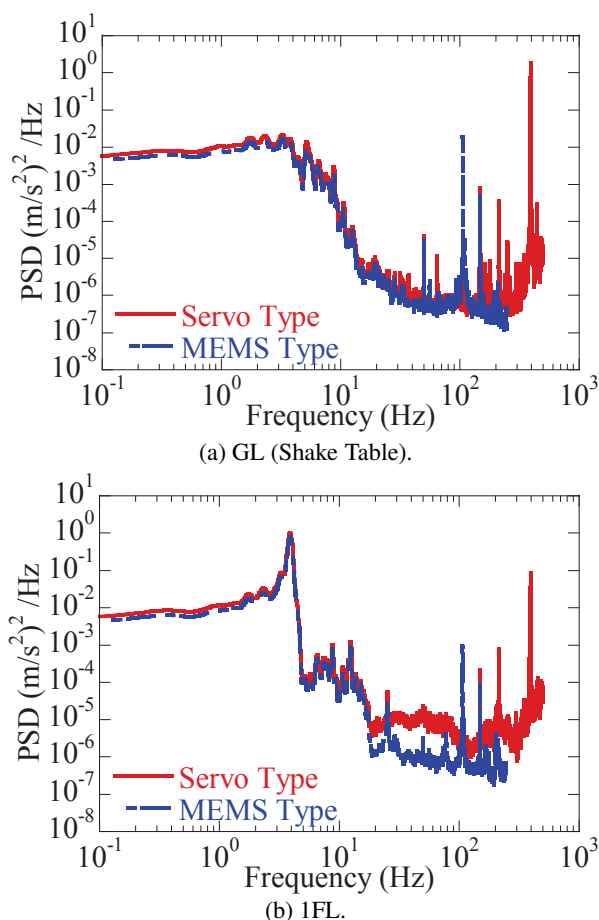


Fig. 4. Acceleration spectrum densities.

sured accelerations after smoothing by a Parzen window with 0.5 Hz band width.

In Fig. 3(a) showing the acceleration measurements on the shake table, the accelerations measured by the servo type accelerometer contain high frequency components that they are larger in values than those measured by the MEMS type accelerometer. As shown in Fig. 4(a), the high frequency components, as measured by the servo type accelerometer, are roughly 400 Hz. Although not shown in Fig. 4(a), other servo type accelerometers on

the shake table present similar responses, suggesting that 400 Hz vibration components have been excited by some other factors such as mechanical vibration. On the other hand, the acceleration measurements by the MEMS type accelerometer show no high frequency components with 400 Hz, because its sampling rate is 500 Hz, for which the Nyquist frequency is 250 Hz. We can see from Fig. 4(a) that the acceleration measurements by the MEMS type accelerometer have large components in 100 Hz, which seem to represent folding noises by the 400 Hz vibration components. Although such folding noises are hard to remove with a digital filter after AD conversion, they can be effectively removed by inserting an analog filter before AD conversion. However, the MEMS type accelerometer, with such a structure as to fulfill AD conversion within its IC and directly output digital signals, cannot remove such folding noises. We also need to pay attention to the vibration components that are outside the range of frequencies measurable with the MEMS type accelerometers.

The response accelerations and their power spectrum densities measured on 1FL, as in Figs. 3(b) and 4(b), show larger components in the vibration components, over 20 Hz, by the servo type accelerometer than by the MEMS type accelerometer. Such differences in acceleration measurements between the servo type and the MEMS type accelerometer may be attributed to differences in the installation locations and methods of the sensors, or to differences in sensitivity of the sensors.

2.3. Measurements of Rotational Components by Gyro Sensors and Error Corrections

Figure 5 shows the angular velocities measured by the MEMS type sensor. We can see from Fig. 5 that the MEMS type sensor rotates at a maximum angular velocity of 2.9 deg/s by 40% excitations and at a maximum angular velocity of 11.8 deg/s by 270% excitations. With the sensor initial inclination set at 0, their trapezoidal integration makes the sensor inclinations as shown in Fig. 6. We can see from Fig. 6, for the sensor responses on 1FL, that its maximum inclination is 0.6 deg.

The sensor inclinations affect the acceleration measurements. Considering that sensors can rotate in any arbitrary directions, there are already a variety of techniques proposed, especially in the field of robotics, for correcting such inclinations and transforming them into a spatial coordinate system [7]. In this paper, sensor inclinations, expressed by quaternions, are corrected by transforming them into a coordinate system. A quaternion represents an expanded complex number of one real number and three imaginary numbers [8].

$$q = q_0 + q_1i + q_2j + q_3k = (q_0; q_1, q_2, q_3), \quad (1)$$

where i, j, k denote imaginary axes.

Inclinations of any arbitrary coordinate axes can be represented by setting a certain rotation axis for orthogonally intersecting coordinate axes and rotating it at a prescribed angle around the designated rotation axis. When it is rotated by θ mainly in the direction of a unit vector

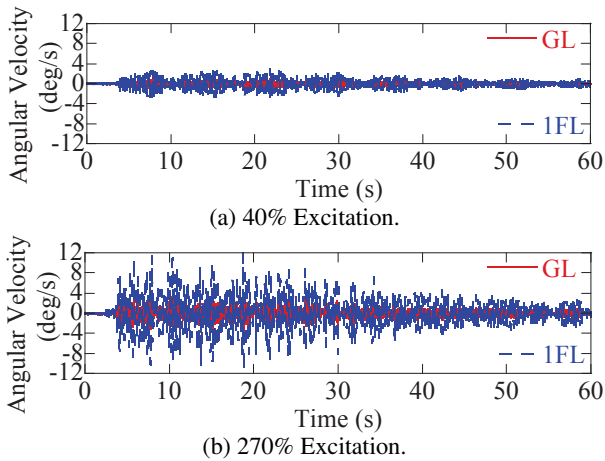


Fig. 5. Measured angular velocities.

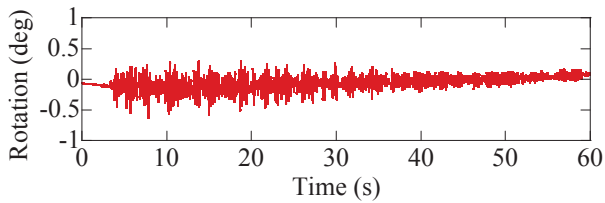


Fig. 6. Sensor's inclinations (1FL, 270% excitation).

$\mathbf{v} = (v_x, v_y, v_z)$, its quaternion is defined by the following equation:

$$q = (\cos \theta; v_x \sin \theta, v_y \sin \theta, v_z \sin \theta). \quad (2)$$

Angular velocities measured by the gyro sensors can be transformed into quaternions by using the following equation [9].

$$\begin{pmatrix} \dot{q}_0 \\ \dot{q}_1 \\ \dot{q}_2 \\ \dot{q}_3 \end{pmatrix} = \frac{1}{2} \begin{bmatrix} q_1 & q_2 & q_3 \\ -q_0 & -q_3 & q_2 \\ q_3 & -q_0 & q_1 \\ -q_2 & q_1 & -q_0 \end{bmatrix} \begin{pmatrix} \omega_x \\ \omega_y \\ \omega_z \end{pmatrix}. \quad (3)$$

A coordinate transformation matrix is generally used for the coordinate transformation of a three-dimensional vector, and quaternions can be easily transformed into the coordinate transformation matrix R.

$$\mathbf{R} = \begin{bmatrix} 1 - 2(q_2^2 + q_3^2) & 2(q_1q_2 + q_0q_3) & 2(q_1q_3 - q_0q_2) \\ 2(q_1q_2 - q_0q_3) & 1 - 2(q_1^2 + q_3^2) & 2(q_2q_3 + q_0q_1) \\ 2(q_1q_3 + q_0q_2) & 2(q_2q_3 - q_0q_1) & 1 - 2(q_1^2 + q_2^2) \end{bmatrix}. \quad (4)$$

Accelerations $(a_{x,m}, a_{y,m}, a_{z,m})$ in a spatial coordinate system can be obtained from the accelerations $(a_{x,a}, a_{y,a}, a_{z,a})$ measured with the above-mentioned coordinate transformation matrix R by using the following equation:

$$\begin{pmatrix} a_{x,a} \\ a_{y,a} \\ a_{z,a} \end{pmatrix} = \mathbf{R} \begin{pmatrix} a_{x,m} \\ a_{y,m} \\ a_{z,m} \end{pmatrix}. \quad (5)$$

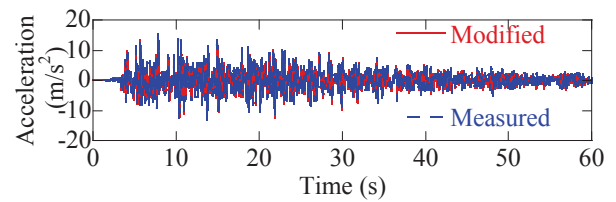


Fig. 7. Accelerations after correcting effects of sensor inclinations (1FL, 270% excitation).

Figure 7 shows the accelerations corrected by Eq. (5) in comparison with the measured ones at a 270% excitation: the maximum accelerations are 15.309 m/s^2 before corrected and 15.228 m/s^2 after corrected. The shake table tests we have conducted in this study show a 0.5% difference in accelerations before and after corrected, which would have no significant effects. In the tests, we have excited vibrations in only one direction, which represents an ideal test condition. In the future, we will need to verify these results under more realistic conditions, for instance, by simultaneous input in three directions.

2.4. Accuracy Verification of Displacement Measurements

Measurements by the wire type sensors cannot neglect errors owing to vibrations of the wire itself. Because the displacements to be measured are relative displacements from the rigid frame assumed as a fixed point, vibrations of the rigid frame can also cause errors.

Vibrations of the wire itself can be evaluated by seeking the natural frequency of the wire with a tension. The natural frequency f of the wire with a tension F_s can be obtained from the following equation by using the wire length L and wire linear density ρ :

$$f = \frac{1}{2L} \sqrt{\frac{F_s}{\rho}}. \quad (6)$$

In this experiment, the distance from the sensor body installed on the rigid frame to the measuring point is 1000 mm, wire tension is about 5–8 N and wire diameter is 0.45 mm. Therefore, wire vibration frequency is 39.1 Hz.

The rigid frame vibrations are evaluated by the averages of an accelerometer installed on it. Fig. 8 shows the transfer function of response acceleration of rigid frame relative to acceleration measured at shake table based on white-noise excitation which is conducted before BCJ-L' record excitation. As shown in Fig. 8, the rigid frame is vibrated with a frequency of approximately 30 Hz. Such vibration components should not be contained in any significant measurements and should better be removed by a low pass filter. Fig. 9 shows the displacement measurements in the shake table tests at 40% and 270% input levels, with a 20 Hz low pass filter to remove errors owing to the natural vibrations of the wire and frame. Fig. 9 shows the displacements enlarged from 10 s to 20 s after the excitation: the fine vibrations have all been removed

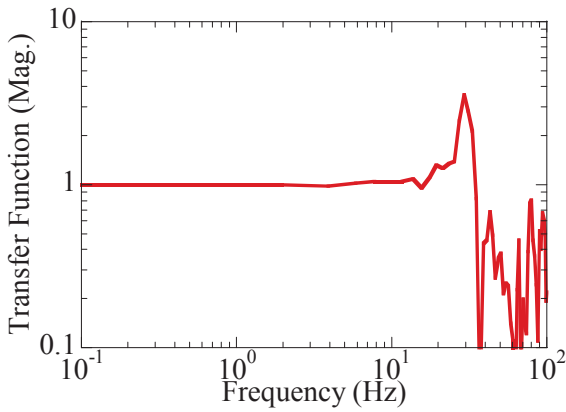


Fig. 8. Transfer function of rigid frame.

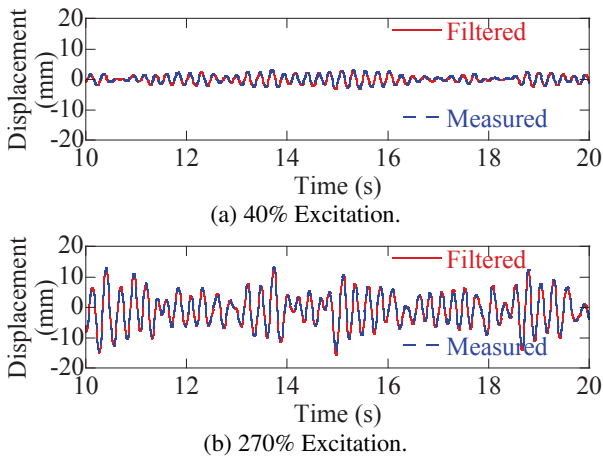


Fig. 9. Displacements after low pass filtering (1FL).

although this is not so clear in Fig. 9. There are generally no changes in responses, suggesting that errors caused by the vibrations of the wire and the frame are not so large.

3. Integration Method Suited to Evaluate Structural Displacement Responses

We integrate the accelerations measured with the MEMS type accelerometer in Fig. 7, in both the time and frequency domains, and compare the integrations with the displacement measurement results described in the preceding Section.

3.1. Integrations in Time Domain

A number of methods have been proposed for integrating accelerations in order to seek displacements. Here we compute the displacements on the following equation of integrations in the time domain.

$$v_{j+1} = v_j + \frac{1}{2} (a_j + a_{j+1}) \Delta t, \quad (7)$$

$$u_{j+1} = u_j + v_j \Delta t + \left(\frac{1}{2} - \beta \right) a_j \Delta t^2 + \beta a_{j+1} \Delta t^2, \quad (8)$$

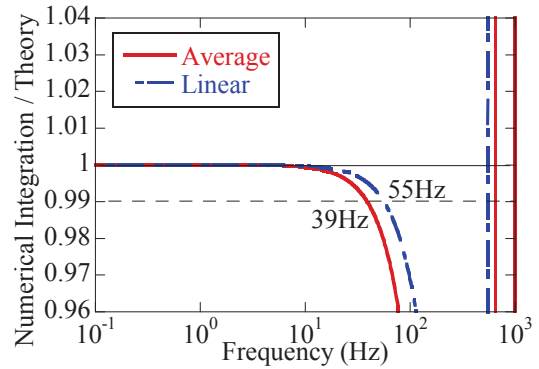


Fig. 10. Ratio of transfer function by numerical integrations to that by theoretical double integrations.

where u_j, v_j, a_j denote displacement, velocity and acceleration respectively in the j th step. As the responses until the j th step have already been all calculated and acceleration in the $(j + 1)$ th step is already known, velocity and displacement in the $(j + 1)$ th step can be obtained from the above equation; Δt denotes a sampling time interval. β denotes a parameter that changes with the assumed temporal changes of accelerations from the j th step to the $(j + 1)$ th step. It is $1/4$ in the average acceleration method where the accelerations in the j th step and $(j + 1)$ th step are assumed constant in average values and $1/6$ in the linear acceleration method where the accelerations change linearly (linear expression) from the j th step to the $(j + 1)$ th step.

We can see from Eqs. (7) and (8) that the displacements can be obtained by integrating accelerations in the time domain, if the computed velocities and displacements in the past time steps and acceleration measurements in the current step are available. Therefore, integrating accelerations in the time domain has a big advantage for seeking responses in real time, although it has some constraints regarding computation time.

In order to grasp the frequency response characteristics of Eq. (8), we seek its transfer function by the averages of Z-transformation. With Z-transformed acceleration a_j and displacement u being denoted by A_j and U_j , respectively, the transfer function of displacement u_j by acceleration a_j is obtained by dividing U_j by A_j as in the following equation:

$$H_j = \frac{U_j}{A_j} = \frac{\beta + (1 - 2\beta)z^{-1} + \beta z^{-2}}{(1 - z^{-1})^2} \Delta t^2. \quad (9)$$

Assuming a sampling rate of 1000 Hz, we have compared the transfer functions of the displacements obtained by the average and linear acceleration methods in Eq. (9) with the transfer functions by theoretical double integrations (Fig. 10). We can see from Fig. 10 that the theoretical solutions and numerical integrations correspond with each other with sufficiently high accuracy in the region of lower frequencies. Further, the numerical integrations tend to get smaller than the theoretical solutions in the region of higher frequencies. When the frequencies

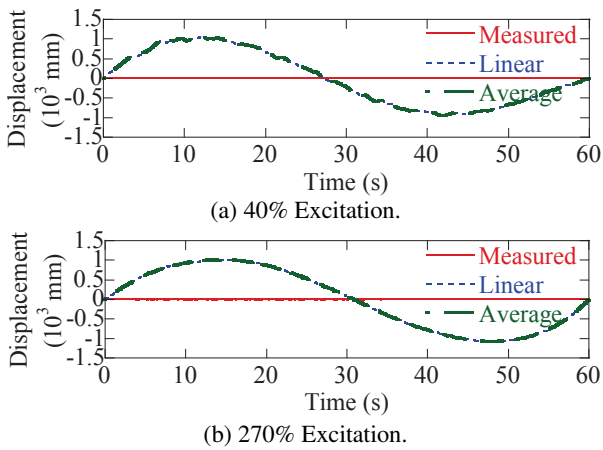


Fig. 11. Calculations of displacements by integrations in time domain.

reach 39 Hz in the average acceleration method and 55 Hz in the linear acceleration method, any difference between the displacements derived by numerical calculations and by theory becomes bigger than 1%. There is some proportionality between the sampling rate and the frequency where the difference in displacements from the theoretical solutions begins to get larger. In the measurements at 100 Hz, for instance, any difference in displacements would exceed 1% at frequencies from 3.9 Hz to 5.5 Hz, which possibly leads us to underestimate the displacements of the evaluation object, depending on its natural frequency. We should take due note of this fact.

Figure 11 shows the displacements obtained by integrating in the time domain the acceleration measurements with the MEMS type displacement sensor in both the average and linear acceleration methods. Displacements directly measured with the wire type sensor are also shown in **Fig. 11** for the sake of comparison. We can clearly see from **Fig. 11** that some of the calculated displacements exceed 1 m, apparently unrealistic solutions that result from excessive amplifications of errors in the long-period components and their diversions. There is no large difference between the average and the linear acceleration methods, both of which have yielded nearly the same solutions.

Figure 12 shows the power spectrum densities of response displacements as obtained by the linear acceleration method. It also shows the power specter densities of displacements as obtained by the wire type displacement sensor for the sake of comparison. We can clearly see from **Fig. 12** that there are large differences in components with a period longer than 0.5 Hz. Such unnaturally large response displacements have been caused by the large differences in the long-period components.

3.2. Integration in Frequency Domain

Here, in order to seek displacements by the Fourier inverse transformation, we integrate the Fourier coefficients to be obtained by the discrete Fourier transformation of accelerations [11]. With the total number of steps being denoted by N , acceleration measured in the j th step by a_j ,

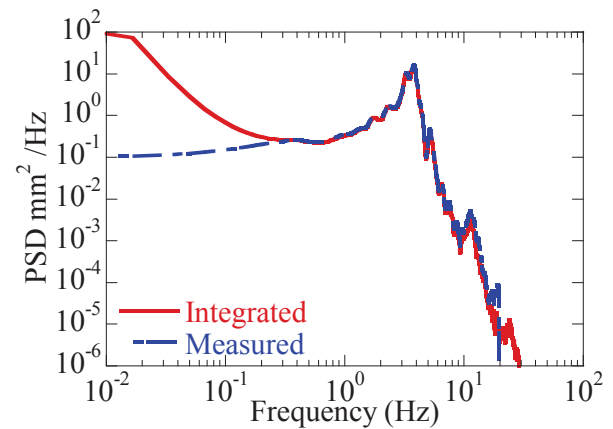


Fig. 12. Power spectrum densities of displacements obtained by double integrations.

displacement to be obtained by u_j , and k^{th} Fourier coefficients of the accelerations and displacements by A_k and U_k , the displacements can be obtained by double integrating the accelerations as in the following equations:

$$A_k = \sum_{j=0}^{N-1} a_j e^{-2\pi i j k / N}, \quad \dots \dots \dots (10)$$

$$U_k = \left(\frac{i k \Delta t}{2\pi N} \right)^2 A_k, \quad \dots \dots \dots (11)$$

$$u_j = \frac{1}{N} \sum_{k=0}^{N-1} U_k e^{2\pi i j k / N}, \quad \dots \dots \dots (12)$$

Equation (10) expresses a Fourier transformation, Eq. (12), a Fourier inverse transformation, and Eq. (11) integrations of accelerations by frequency component.

As clearly seen from Eqs. (10) and (12), unless acceleration measurements in all time steps are available, they cannot be decomposed into frequency components and thus the proposed method cannot be applied. However, the proposed method enables us obtain acceleration in high vibration components more accurately without generating such errors from the theoretical solutions, as in **Fig. 9** in the high vibration components. Although as the total number of steps increases the calculation costs rise at an increasing tempo, recent progress in computing technology has made discrete Fourier transformation costs less problematic.

Figure 13 shows the displacements obtained by integrating the acceleration measurements by the MEMS type accelerometer in the frequency domain. For the sake of comparison, it also shows the displacements obtained by integrating the accelerations in the time domain. We can see from **Fig. 13** that error in the long-period components are greatly amplified for both the cases where they are integrated in the frequency domain and they are integrated in the time domain.

Although not shown here, power spectrum densities would present large errors in the long-period components, as is the case with the result in **Fig. 12**, generating unrealistic large displacements.

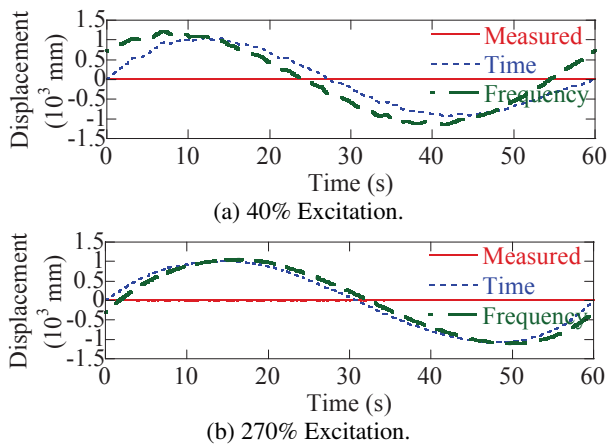


Fig. 13. Calculations of displacements by integrations in frequency domain.

3.3. Removal of Errors in Long-Period Components by High Pass Filter

As described above, displacements excessively increase to an unrealistic extent by the effects of errors in the long-period components. Therefore, we attempt to remove apparent errors in the long-period components by a high pass filter, as previous studies have done. In the high pass filtering process, we have removed long-period components by setting to 0 any Fourier coefficients less than a cut-off frequency in the Fourier coefficients obtained by the discrete Fourier transformation so that no phase delays should be caused by the filtering process.

Then, we need to decide how to set such a cut-off frequency that will determine the extent of the frequency band to be removed. In this study, we have used the correlation coefficients as an indicator to determine an optimum cut-off frequency. When there is a linear relationship between two indicators and its inclination is positive, the correlation coefficient becomes 1. Thus, any cut-off frequencies whose correlation coefficients are closer to 1 would very likely be able to properly evaluate displacement responses. We should take care, however, that when an indicator is expressed by a constant multiplication of another indicator, their correlation coefficient will become 1, and that a correlation coefficient of 1 does not always indicate that they are identical in waveforms.

We have first obtained the correlation coefficients between the displacements obtained with varying cut-off frequencies and the measured displacements. **Fig. 14** shows the relations between cut-off frequencies and such correlation coefficients. **Fig. 14(b)** shows, for the sake of comparison, the transfer function of the accelerations measured with the MEMS type accelerometer at the height of 1FL in relation to the point on the vibration table. We can see from **Fig. 14** that as the excitation level is higher, the cut-off frequency with a high correlation coefficient gets lower, indicating that the natural frequency of the specimen is involved in some way.

With 40% excitation, there is a small range of cut-off frequencies with high correlation coefficients, probably

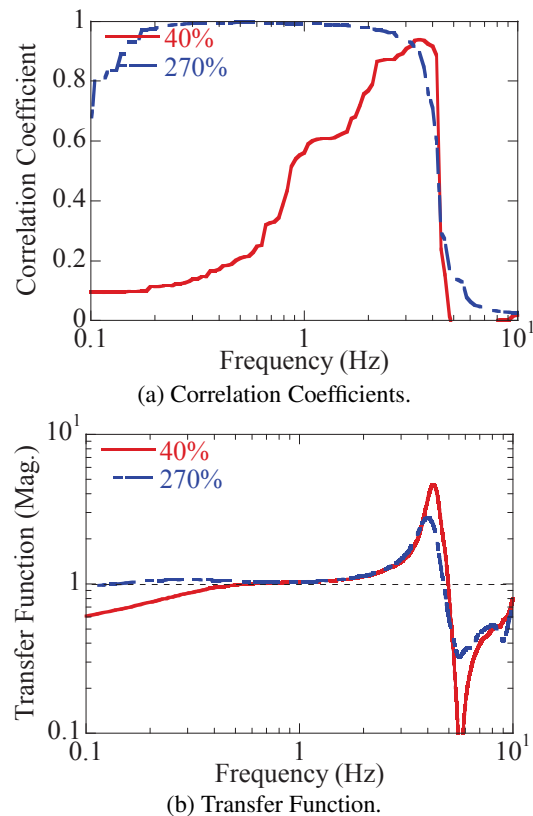


Fig. 14. Relations between cut-off frequencies and correlation coefficients and test-piece natural frequency.

because such a low input level and resultant low responses have led to relatively large errors.

Figure 15 shows the relations between the maximum cut-off frequency with a correlation coefficient R larger than 0.85, as obtained from **Fig. 14(a)**, and the natural frequency of the specimen as obtained from **Fig. 14 (b)**. It also shows our past research results, in which we have evaluated, in the same way as in this paper, the responses measured at the roof top of a full-scale steel gymnasium specimen. This was subjected to a shake table test conducted using the E-Defense world's largest shake table facility [12]. The above-mentioned results of this study, which extrapolates the past research results, prove that response displacements can be evaluated with sufficient accuracy if the cut-off frequency is up to 90% of the natural frequency of the specimens. Even when the natural frequency of the specimen is slightly changed due to plastic deformation, if we evaluate the natural frequency in the same way and seek the vibration frequencies that will provide predominant responses, we just have to select a cut-off frequency smaller than 90% of the natural frequency and then remove the long-period components by a high pass filter in the integral operations. Note that further study is needed for evaluation of appropriate cut-off frequency for high pass filter to the structures with rupture or some other significant damage to a lot of members. In such a case, however, we will be able to see, without any monitoring, that the structure is so heavily damaged

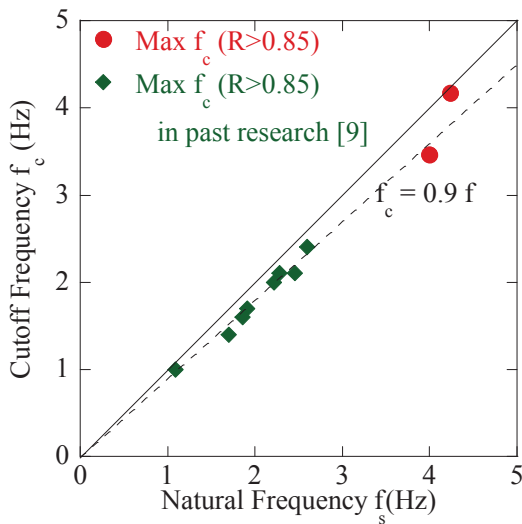


Fig. 15. Relations between natural frequency and cut-off frequency with high correlation coefficient.

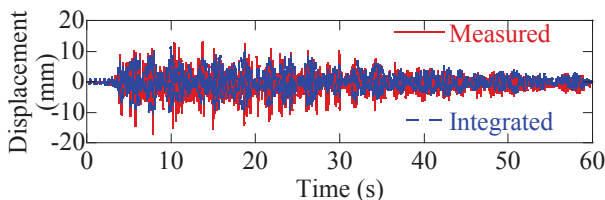


Fig. 16. Response displacements obtained by double integrations (270% excitation).

that it is in a dangerous state. Thus, monitoring would be less necessary and this should not necessarily be a disadvantage.

Figure 16 shows the response displacements obtained with a high pass filter of 3.6 Hz, equivalent to 0.9 of the natural frequency of specimen. Although it provides generally slightly smaller responses, they represent generally accurate evaluations.

4. Conclusion

To evaluate the performance of MEMS (Micro Electro Mechanical Systems) type accelerometers and double integration method of acceleration for displacement, the small scaled steel frame specimen is excited using “Large-scale earthquake simulator” belonging to the National Research Institute for Earth Science and Disaster Resilience (NIED). The conclusions arrived at in this study is summarized as follows:

- We have found that the MEMS type accelerometer used for the experiment in this study can provide nearly the same responses as the conventional servo type accelerometer that is widely used to monitor buildings in the frequency bands of 100 Hz or less. The MEMS type accelerometer has such performance that it can also be applied for monitoring buildings.

- While analog filters are effective in removing folding noises owing to vibrations in a range exceeding the Nyquist frequency that can be obtained from the sampling rates, the MEMS type accelerometer has such a structure that allows its measurements to be directly provided in digital signals. We should note that it is difficult to tune by analog channels according to individual situations.
- The integrations of the angular velocities measured by the MEMS type sensor have revealed that the sensor has rotated by about 0.6 deg at the maximum. We have corrected the measurement errors owing to the sensor inclination by a coordinate transformation with quaternions, which has resulted in a reduction of the size of measurement errors to about 1%.
- In obtaining displacements by double integrating the recorded accelerations, the amplitudes of high frequency components are attenuated in the integrations in the time domain. Errors of 1% or more are generated in relation to the theoretical solutions at 39 Hz in the average acceleration method and at 55 Hz in the linear acceleration method, for a sampling rate of 1000 Hz. As the sampling rate decreases, such attenuations also occur in lower frequency regions. We need to grasp in advance the vibration characteristics of an object structure, including higher order modes, so that we can carry out high-speed measurements as much as possible.
- Double integrations of the recorded accelerations have resulted in unrealistically response displacements, owing to errors of the long-period components. Such errors can be effectively removed by a high pass filter. As the optimum cut-off frequency depends on the vibration characteristics of an object structure, we have proved that sufficiently accurate response displacements can be obtained if the cut-off frequency is up to 0.9 of the natural frequency.

Acknowledgements

This study has been financially supported by the JSPS KAKENHI Grant Number 24760463 and by the Management Expenses Grants of the National Institute for Earth Science and Disaster Resilience. We express our hearty thanks to all those who have kindly assisted us in carrying out the tests.

References:

- [1] C. R. Farrar and K. Worden, “An Introduction to Structural Health Monitoring,” *Philosophical Trans. of the Royal Society A*, Vol.365, pp. 303-315, 2006.
- [2] J. P. Lynch, “An Overview of Wireless Structural Health Monitoring for Civil Structures,” *Philosophical Trans. of the Royal Society A*, Vol.365, pp. 345-372, 2006.
- [3] J. P. Lynch and K. J. Koh, “A Summary Review of Wireless Sensors and Sensor Networks for Structural Health Monitoring,” *The Shock and Vibration Digest*, Vol.38, No.2, pp. 91-128, 2006.
- [4] M. D. Trifunac, “Zero Baseline Correction of Strong-Motion Accelerograms,” *Bulletin of the Seismological Society of America*, Vol.61, No.5, pp. 1201-1211, 1971.

- [5] G. V. Berg and G. W. Housner, "Integrated Velocity and Displacement of Strong Earthquake Ground Motion," *Bulletin of the Seismological Society of America*, Vol.51, No.2, pp. 175-189, 1961.
- [6] T. Yamashita, "Preliminary Analysis for Shake Table Test of Small-Scaled Steel Frame Using Detailed FEM," *Summaries of Technical Papers of Annual Meeting 2016 (Structure III)*, AIJ, pp. 701-702, 2016 (in Japanese).
- [7] K. Hirose and A. Kondo, "Special Issues No.3 Measurement Technique for Ergonomics, Section 1-2 Measurement of Body Motion – Motion Measurements by Inertial Sensors –," *J. of Japan Ergonomics*, Vol.50, No.4, pp. 182-190, 2014 (in Japanese).
- [8] W. R. Hamilton, "On Quaternions; or on a New System of Imaginaries in Algebra," *Philosophical Magazine*, Vol.25, No.3, pp. 489-495, 1844.
- [9] A. M. Sabatini, "Quaternion-Based Extended Kalman Filter for Determining Orientation by Inertial and Magnetic Sensing," *IEEE trans. on Biomedical Engineering*, Vol.53, No.7, pp. 1346-1356, 2006.
- [10] Y. Ohsaki, "New Introduction of Spectrum Analysis for Earthquake," *Kajima Institute Publishing*, ISBN 9784306032705, 1994 (in Japanese).
- [11] A. Papulis, "The Fourier Integral and Its Applications," McGraw-Hill, 1962.
- [12] T. Sasaki, D. Sato, R. Suzuki, H. Tagawa, A. Aoi, and K. Kajiwara, "Verification of Displacement Integrated from Measured Acceleration on Shake Table Experiment of Full-Scale Gymnasium Specimen," *AIJ J. Technol. Des.* Vol.23, No.54, pp. 427-432, Jun., 2017 (in Japanese).



Name:
Tomohiro Sasaki

Affiliation:
Senior Researcher, Hyogo Earthquake Engineering Research Center, Earthquake Disaster Mitigation Research Division, National Research Institute for Earth Science and Disaster Resilience (currently Technical Research Institute, Obayashi Corp.)

Address:
1501-21 Mitsuta, Shijimi-cho, Miki, Hyogo 673-0515, Japan

Brief Career:
2011- Associated Research Fellow, NIED
2016- Senior Researcher, NIED
2017- Researcher, Technical Research Institute of Obayashi Corp.

Selected Publications:

- T. Sasaki, K. Kawashima, G. Watanabe, S. Nagata, K. Tharin, H. Ukon, and K. Kajiwara, "Effect of Loading Protocols on Premature Shear Failure of Reinforced Concrete Bridge Piers with Termination of Main Reinforcements," *J. of Structural Engineering*, JSCE, Vol.53A, pp. 449-460, 2007.
- T. Sasaki, A. Aoi, H. Tagawa, K. Kajiwara, D. Sato, T. Kabeyasawa, T. Seike, S. Yamada, and H. Fukuyama, "Design and Structural Response of Full-scale Steel Gymnasium Specimen E-Defense shake table experiment on collapse mechanism of wide-area suspended ceiling in gymnasium part 1," *J. of Structural and Construction Engineering (Trans. of AIJ)*, AIJ, Vol.82, No.736, pp. 831-841, 2017 (in Japanese).

Academic Societies & Scientific Organizations:

- Japan Society of Civil Engineers (JSCE)
- Architectural Institute of Japan (AIJ)
- Japan Association of Earthquake Engineering (JAEE)



Name:
Koichi Kajiwara

Affiliation:
Director-General, Hyogo Earthquake Engineering Research Center, Earthquake Disaster Mitigation Research Division, National Research Institute for Earth Science and Disaster Resilience (NIED)

Address:
1501-21 Mitsuta, Shijimi-cho, Miki, Hyogo 673-0515, Japan

Brief Career:
2000- Senior Research Officer, NIED
2010- Deputy Director-General, NIED
2011- Director-General, NIED

Selected Publications:

- R. Enokida and K. Kajiwara, "Nonlinear Substructuring Control for Parameter Changes in Multi-Degree-of-Freedom Systems," *J. of Sound and Vibration*, Vol.407, pp. 63-81, 2017.
- R. Enokida and K. Kajiwara, "Nonlinear Signal-Based Control with an Error Feedback Action for Nonlinear Substructuring Control," *J. of Sound and Vibration*, Vol.386, pp. 21-37, 2017.

Academic Societies & Scientific Organizations:

- Architectural Institute of Japan (AIJ)
- Japan Society of Mechanical Engineers (JSME)
- Japan Society of Civil Engineers (JSCE)



Name:
Takuzo Yamashita

Affiliation:
Senior Researcher, Hyogo Earthquake Engineering Research Center, Earthquake Disaster Mitigation Research Division, National Research Institute for Earth Science and Disaster Resilience (NIED)

Address:
1501-21 Mitsuta, Shijimi-cho, Miki, Hyogo 673-0515, Japan

Brief Career:
2010- Associated Research Fellow, NIED
2012- Researcher, NIED
2016- Senior Researcher, NIED

Selected Publications:

- T. Yamashita, T. Miyamura, T. Ogawa, and T. Kumagai, "Acceleration of Three-Dimensional Large Eddy Simulation around Cylindrical Roofs Using Multigrid Method with Plural Two-Dimensional Coarse Meshes," *J. of Structural and Construction Engineering (Trans. of AIJ)*, AIJ, 2017 (in press).
- T. Yamashita, M. Ohsaki, M. Kohiyama, T. Miyamura, J. Zhang, and H. Tagawa, "Detailed Finite Element Analysis of Composite Beam under Cyclic Loads," *J. of Structural and Construction Engineering (Trans. of AIJ)*, AIJ, Vol.79, No.704, pp. 81-1490, 2014.

Academic Societies & Scientific Organizations:

- Architectural Institute of Japan (AIJ)
- Japan Society for Computational Engineering and Science (JSCES)
- Japan Society of Civil Engineers (JSCE)



Name:

Takuya Toyoshi

Affiliation:

Associated Research Fellow, Hyogo Earthquake Engineering Research Center, Earthquake Disaster Mitigation Research Division, National Research Institute for Earth Science and Disaster Resilience (NIED)

Address:

1501-21 Mitsuta, Shijimi-cho, Miki, Hyogo 673-0515, Japan

Brief Career:

2016- Associated Research Fellow, NIED

Selected Publications:

- T. Toyoshi, Y. Wada, and T. Furukawa, "Resolution of Measurement by Integrated Centroid Tracking Method (1st Report, Strain Measurement of Static Tensile Test)," Trans. of the Japan Society for Computational Engineering and Science, JSCES, Vol.2015, p. 20150010, 2015.
- T. Toyoshi, Y. Wada, and T. Furukawa, "Camera Calibration Method for Accurate Full-field Strain Measurement by Dot Centroid Method," ASME, DETC2012/CIE-70681, pp. 959-966, 2012.

Academic Societies & Scientific Organizations:

- Architectural Institute of Japan (AIJ)
 - Japan Society for Computational Engineering and Science (JSCES)
 - Japan Society of Mechanical Engineers (JSME)
 - Japanese Society for Experimental Mechanics (JSEM)
-